Jicheng Xia
e-mail: xiaxx028@umn.edu

William K. Durfee[1]
e-mail: wkdurfee@umn.edu

Department of Mechanical Engineering,
University of Minnesota,
111 Church Street SE,
Minneapolis, MN 55455

Analysis of Small-Scale Hydraulic Actuation Systems

We investigated small-scale hydraulic power actuation systems using a system level analysis, where small-scale refers to systems generating 10 to 100 W output power, to determine whether the high power density advantage of hydraulics holds at small sizes. Hydraulic actuator system power density was analyzed with simple physics models and compared to an equivalent electromechanical system comprised of off-the-shelf components. Calculation results revealed that high operating pressures are needed for small-scale hydraulics to be lighter than the equivalent electromechanical system. The analysis was limited to the actuator and conduit as those are the components that must be located on the mechanism. A complete comparison should add the weight and efficiency of the power supply. [DOI: 10.1115/1.4024730]

1 Introduction

Hydraulic fluid power systems are well known for their high power density [1,2]. This advantage is best illustrated in applications such as excavators and heavy manufacturing equipment that require extremely large power and force. Hydraulics is the only practical way to attain these levels of force and power while at the same time being relatively light weight compared to the equivalent electromechanical system. One reason for the high power density of hydraulics is that fluid power cylinders are inherently low-velocity, high-force actuators, which is a good match to the requirements for construction, agricultural and manufacturing heavy equipment. Contrast this with electric motors, which are high-velocity, low torque actuators, that require a transmission such as a gear head or a lead screw to match their optimal operating point to the application. At high forces and torques, the weight of the transmission ends up being a significant fraction of the actuator package weight. A second reason for the high power density is that exceptionally high pressures can be generated. For example, the hydraulic pistons on an excavator operate as high as 380 bar (5500 psi).

An advantage of hydraulics is that the source of pressurized fluid can be housed in a base station and flexible hoses used to transport the fluid to light weight cylinders located at the periphery of the machine. For example, an excavator has actuators to control the boom, stick, and bucket with bulky power supply, reservoir and accumulators placed in the house. The proximal actuators carry the load of the distal. When the excavator arm is fully extended, the bucket actuator at the end of the arm causes large moments at the joint connecting the boom to the house, which requires a powerful boom actuator. If the bucket actuator is a cylinder, the weight of the actuator is small compared to the bucket. If the bucket actuator is electromechanical, the weight of the electric motor and its associated transmissions, both of which must be placed at the joint, can be significant.

The power density of electromechanical systems has an upper limit because of inherent characteristics such as magnetic saturation. In contrast, the power density of hydraulic systems has no inherent upper limit and can be increased by simply increasing the pressure. The maximum power density in a hydraulic system is largely determined by the design of the containing structures and the seals.

There has been recent interest in portable, wearable powered systems including powered exoskeletons and powered orthotics [3,4]. Examples of mobile systems in the 10 to 100 W range include ankle foot orthotics, small robots, and powered hand tools. These devices are usually powered by electromechanics, typically a lithium-ion battery, DC motor, and transmission. Little work has been done on using hydraulics for these applications because off-the-shelf tiny hydraulic components do not exist.

Love [5] demonstrated an application of small scale hydraulics by prototyping a prosthetic finger. Pressure as high as 138 bar (2000 psi) was used to operate 4 mm hydraulic cylinders. Another example is a novel endoscope [6]. Two systems were studied, hydraulics and electric. The results showed that the hydraulic system had larger output force for the same space.

A barrier for increased hydraulic power density at reasonable efficiency is the seals. Too tight and friction dominates. Too loose and the pressurized fluid will leak past the seal. Volder *et al*. developed a ferrofluid seal for microactuators that was able to seal to 1.6 MPa (230 psi) without leakage [7,8], but this approach does not work at higher pressures.

While microfluidics have advanced, they do not inform our problem as microfluidic systems operate well under 1 W and our systems of interest are 10 to 100 W. Reviews of microfluidics components are given in Refs. 9–11. As shown in Ref. 11, micro fluid power cylinders can generate 1 to 10 N, but their strokes are under 10 mm.

Designers might choose hydraulics for tiny, mobile powered systems because the same power density advantage of hydraulics over electromechanical should hold for a powered orthosis as it holds for an excavator. The story, however, is complex because the scaling laws are not intuitive. For example, in a cylinder, force is proportional to area while weight is proportional to volume. Surface effects such as friction drag of seals and viscous drag of gaps become significant at small bores and impact overall efficiency. On the other hand, the thickness, and thus the weight, of a cylinder wall required to contain a fixed pressure goes down with bore. The final weight of a hydraulic system at small scale cannot be determined by proportionally scaling the weight of a large system and determining for equal efficiency, which is lighter a fluid power or an electromechanical system for a tiny system cannot be answered using intuition.

The aim of this study was to use first principles to understand how the weight and other properties of hydraulic systems change with size and to answer the question, "When is a hydraulic solution lighter than an electromechanical solution for tiny, powered systems?" Our goal was to provide guidelines that mechanical designers could use at the early stages of evaluating architectures

[1]Corresponding author.

Contributed by the Mechanisms and Robotics Committee of ASME for publication in the Journal of Mechanical Design. Manuscript received January 11, 2012; final manuscript received May 5, 2013; published online July 2, 2013. Assoc. Editor: Alexander Slocum.

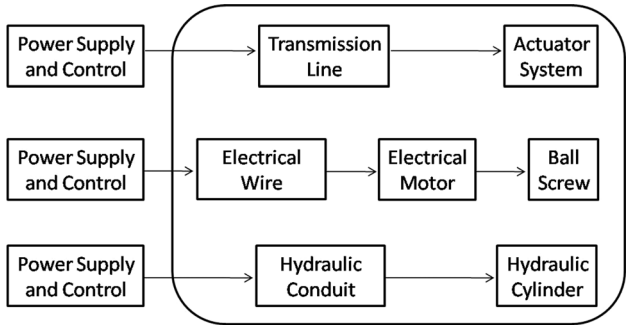

Fig. 1 Architecture for powered actuation system. Top row is generic, middle row is electromechanical, bottom row is hydraulic.

for small systems. Empirical and analytical equations were used to model hydraulic and electromechanical systems, connecting the methods to real components wherever possible. The result of the analysis showed that for equal output power and system efficiency, a hydraulic solution will be lighter than an electromechanical solution only if the hydraulic system operates at high pressure.

2 Benchmark System

The top row of Fig. 1 illustrates the architecture of a generic mobile actuation system that contains a power supply, a means of control, a transmission line and an actuator located at the end-point. For this study, we considered systems that delivered force and velocity along a linear axis. For example, this could be a powered knee prosthesis with the joint driven by a linear actuator mounted behind the knee or a tiny powered gripper driven by a linear actuator.

The electromechanical realization (middle row of Fig. 1) includes a battery power supply, a PWM motor controller, wire, a brushed or brushless DC electric motor and a ball screw to convert the high velocity, low torque output of the motor to a low velocity, high force linear output. The ball screw was chosen because it is lighter and more efficient than the equivalent gear box, and it converts rotary to linear motion, which provides a fair comparison to the hydraulic system. The hydraulic version (bottom row of Fig. 1) includes a battery or internal combustion engine driven pump to generate pressured fluid, a servovalve, pipe or hose and a hydraulic cylinder. Other realizations are possible.

Our analysis only considered the transmission line plus actuator system, the circled components in Fig. 1. These are the parts of the system that must be located at the point of mechanical output where weight is of greatest concern. For example, for a portable hand tool, the power supply and control can be placed in a backpack or tool belt, but the transmission line and actuator system must be held in the hand. In a real mobile system, the power supply will contribute significantly to the weight and in a real system, the control means will contribute significantly to the efficiency. Comparing electromechanical and hydraulic endpoint components, however, still provides valuable information to the designer looking to minimize weight at the endpoint.

3 Hydraulic System Analysis

The objective of the hydraulic system analysis was to estimate the weight of an ideal hydraulic cylinder plus the weight of ideal conduit to predict the total weight for a hydraulic system that delivers a specified mechanical force and power output. The weight of components was estimated from a set of theoretical equations developed using basic physics of fluids and solid mechanics.

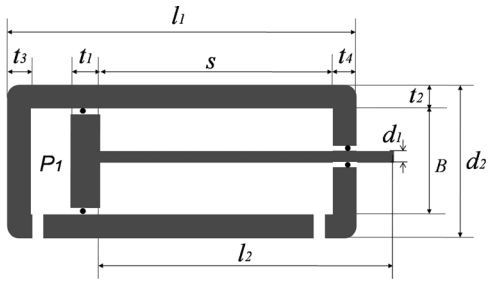

Fig. 2 Ideal hydraulic cylinder used for analysis

3.1 Hydraulic Cylinder. The simplified hydraulic cylinder used for analysis is illustrated in Fig. 2 and its associated parameters are defined in Table 1. The cylinder has bore B, stroke S, and rated maximum pressure P_r. The piston is a disk of uniform thickness t_1 and the cylinder housing is a capped tube with barrel wall thickness t_2 and end cap thicknesses t_3 and t_4. O-ring seals are assumed for piston and rod. While large hydraulic cylinders use a layered arrangement of cup and backing seals, for tiny cylinders, a simple O-ring is an appropriate design choice. Only uni-direction extension motion is considered with cap side pressure P_1 and rod side pressure zero.

3.1.1 Cylinder and Piston Wall Thickness. The pressure loading scenario to calculate the required cylinder wall and the piston thickness is shown in Fig. 3 where the cylinder rated pressure P_m acts everywhere on the wall. The end wall calculations assumed a fixed displacement boundary condition along the end wall circumference. The piston thickness calculation assumed that the rod was fixed and the P_m was distributed uniformly across the cap side of the piston and zero pressure on the rod side. These are all worst-case loading conditions.

The cylinder circumferential wall thickness was calculated using the equation for a thin-walled pressure vessel [12]

$$t_2 = \frac{N \cdot P_m \cdot B}{2S_y} \tag{1}$$

which is valid for $t_2 < B/6$. The cylinder end wall thicknesses t_3 and t_4, and the piston thickness t_1 were calculated using thin plate formulas [13]

$$t_1 = \sqrt{\frac{3NP_mG_1\nu}{4S_y}} \tag{2}$$

Table 1 Hydraulic cylinder parameters

VAR	Description	Unit
B	bore	m
S	stroke	m
l_1	cylinder length	m
l_2	rod length	m
t_1	piston thickness	m
t_2	cylinder circumferential wall thickness	m
t_3	left end wall thickness	m
t_4	right end wall thickness	m
d_1	rod diameter	m
d_2	outer diameter	m
P_m	maximum allowable fluid pressure	Pa
P_1	cylinder left chamber pressure	Pa
S_y	cylinder material yield strength	Pa
E	cylinder material Young's modulus	Pa
ρ	cylinder material density	Kg/m^3
ν	cylinder material Poisson's ratio	—
N	design safety factor	—

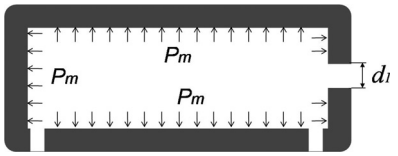

Fig. 3 Wall loading scenario used to calculate wall thickness

$$t_3 = \sqrt{\frac{3\pi B^2 N P_m (1+\nu)}{32\pi S_y}} \tag{3}$$

$$t_4 = \sqrt{\frac{3NP_m G_2}{4\nu S_y}} \tag{4}$$

where G_1 and G_2 are

$$G_1 = \frac{4B^4(1+\nu)\log\frac{B}{d_1} + 4\nu B^2 d_1^2 + d_1^4(1-\nu) - B^4(1+3\nu)}{4\nu(B^2 - d_1^2)}$$

$$G_2 = \frac{d_1^4(1-\nu) - 4d_1^4(1+\nu)\log\frac{B}{d_1} + B^2 d_1^2(1+\nu)}{4B^2(1-\nu) + 4d_1^2(1+\nu)} + \frac{B^2}{4} - \frac{d_1^2}{2}$$

The thin plate formulas are valid for plate thickness that are less than 1/4 of the plate diameter. The formula used to determine t_4 was that for a round plate containing a central hole.

Using the material yield strength to determine the minimum thickness of a cylinder is a simplification. For larger cylinders, expansion of the cylinder when pressurized due to the elasticity of the material matters because a slight increase in bore will cause leakage past the piston seal. Therefore, it is common practice to design walls that are thick enough for the expansion to be insignificant. As the bore size decreases, so does the expansion so for tiny cylinders with thin walls the increased leakage is insignificant.

3.1.2 Rod Diameter. The rod must be sized so that it will not buckle under the maximum compressive load. The required rod diameter was calculated using Euler and JB Johnson buckling formulas [13], assuming that the rod was fully extended, loaded in compression and carrying the piston force at the maximum rated pressure. The slenderness ratio $\frac{l_2}{\rho_1}$ dictates whether the Euler or the JB Johnson formula is appropriate. The critical rod slenderness ratio is

$$\left(\frac{l_2}{\rho_1}\right)_{\text{crit}} = \sqrt{\frac{2\pi^2 E}{S_y}} \tag{5}$$

where $\rho_1 = d_1/4$ for a solid round rod. For a slenderness ratio less than the critical value the JB Johnson formula was used

$$d_1 = \sqrt{\frac{4NP_m\pi(B/2)^2\eta_f}{\pi S_y} + \frac{S_y l_2^2}{2\pi^2 E}} \tag{6}$$

and for other cases, the Euler formula was used

$$d_1 = \left(\frac{32Nl_2^2 P_m \pi (B/2)^2 \eta_f}{\pi^3 E}\right)^{\frac{1}{4}} \tag{7}$$

3.1.3 Cylinder Efficiency. The force in the rod is less than the pressure times the area of the piston because of the friction in the piston and rod seals. The cylinder force efficiency, η_f is

$$\eta_f = \frac{F_r}{P_1 A_1} \tag{8}$$

Table 2 Symbols used in Eqs. (10) and (11)

VAR	Description	Unit
F_s	friction force piston with seal	N
f_s	O-ring seal friction coefficient	—
D	piston or rod diameter	m
d	O-ring cross-sectional diameter	m
E_s	O-ring Young's modulus	Pa
ε	O-ring squeeze ratio	—
Q_s	leakage across sealed piston or rod	m^3/s
μ	hydraulic fluid dynamic viscosity	Pa · s
U_{hc}	piston velocity	m/s
δ_m	maximum O-ring contact stress	Pa
s_0	O-ring contact width	m

where F_r is the rod compressive force, P_1 is the cap side pressure, and A_1 is the cap side piston area [14].

The velocity of the rod is less than the flow divided by the area of the piston because of the leakage through the piston and rod seals. The cylinder volumetric efficiency, η_q is

$$\eta_q = \frac{V_r}{Q/A_1} \tag{9}$$

where V_r is the rod velocity and Q is the flow into the cylinder [14].

Equations (10) and (11) are approximations that describe the seal friction [15] and leakage [16,17] for a rubber O-ring seal with variables defined in Table 2

$$F_s = f_s \cdot \pi \cdot D \cdot d \cdot E_s \cdot \varepsilon \cdot \sqrt{2\varepsilon - \varepsilon^2} \tag{10}$$

$$Q_s = 2.99 \cdot \pi \cdot D \cdot \mu^{0.71} \cdot U_{\text{hc}}^{1.71} \cdot \delta_m^{-0.71} \cdot s_0^{0.29} \tag{11}$$

As described in Refs. 15–17, the effect of pressure across the seal appears through f_s, which varies with pressure because the O-ring tends to extrude into the gap at higher pressure causing higher friction, and in the δ_m and s_0 terms for leakage.

Applying Eqs. (10) and (11) for the piston and the rod yields the estimation of the cylinder force, volumetric and overall efficiency

$$\eta_f = \frac{P_1 A_1 - F_{sp} - F_{sr}}{P_1 A_1} \tag{12}$$

$$\eta_q = \frac{V_r A_1}{V_r A_1 + Q_{sp} + Q_{sr}} \tag{13}$$

$$\eta_{\text{hc}} = \eta_f \cdot \eta_q \tag{14}$$

where F_{sp} is piston seal friction force, F_{sr} is rod seal friction force, V_r is rod velocity, Q_{sp} is piston seal leakage, and Q_{sr} is rod seal leakage.

As shown in Fig. 4, cylinder efficiency is a strong function of bore size for smaller cylinders. This is because friction and leakage are a function of piston diameter while force and flow are a function of piston area.

3.1.4 Cylinder Weight. The volume of the cylinder is

$$V_{\text{cyl}} = \frac{\pi}{4}[(d_2^2 - B^2)l_1 + B^2(t_3 + t_1 + t_4) + d_1^2 l_2 - \Delta_V] \tag{15}$$

where Δ_V are the adjustments to the volume due to the inlet, outlet, and rod openings. For simplicity, only the rod opening volume will be included as the inlet and outlet openings is balanced by the volume of fittings

$$\Delta_V = d_1^2 \cdot t_4 \tag{16}$$

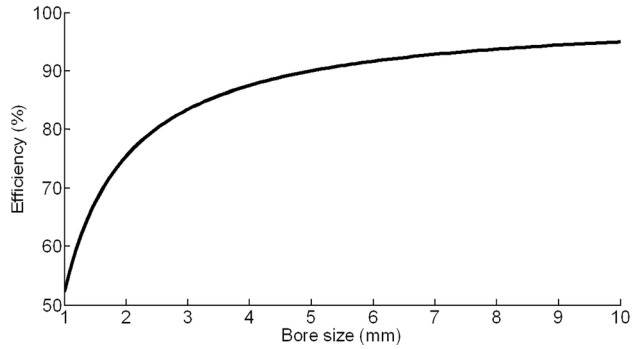

Fig. 4 Cylinder efficiency as a function of bore size. The plot was generated assuming 500 psi operating pressure and 0.1 m/s rod speed.

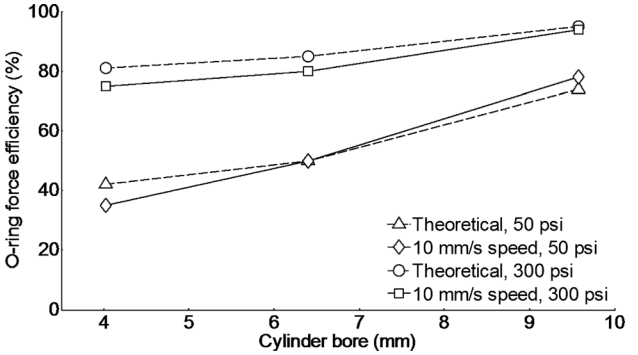

Fig. 6 Experimentally determined cylinder force efficiency as a function of cylinder bore and two rod speeds. Overlaid are the equivalent results from the O-ring model.

Assuming the same material is used for the cylinder wall, piston and rod, the weight of the cylinder is

$$M_{\text{cyl}} = \rho \cdot V_{\text{cyl}} \tag{17}$$

3.1.5 Validation. To validate the O-ring friction (10) and leakage (11) models, a test stand was built to collect corresponding experimental data for 4, 6, and 9 mm cylinders. A single O-ring seal was mounted on a ram, which was used to raise a constant load. The cylinder chamber underneath the ram was pressurized by a small hydraulic pump. When the cylinder reached full extension, the pump was shut off and a needle valve cracked to create different ram descending speeds at constant chamber pressure. The chamber pressure and the ram speed were sensed by a pressure transducer and a linear potentiometer whose output was conditioned and sampled at 100 Hz.

The comparison between the measured and the theoretical O-ring force efficiency for the 9 mm bore cylinder is shown in Fig. 5 and is representative of the data for the 6 mm and 4 mm cylinders. In Fig. 5, the minimum and maximum theoretical efficiency lines were generated using the maximum and the minimum reasonable friction coefficient f_s between the O-ring and the cylinder wall. The higher piston speeds resulted in higher efficiency, which indicates that the lubrication between the O-ring and the cylinder wall shifted from mixed lubrication to hydrodynamic lubrication as the piston speed changed from 1 mm/s to 20 mm/s. Figure 6 demonstrates that the O-ring force efficiency model is valid for different bore sizes and different chamber pressures.

Because leakage model (11) predicts essentially zero leakage for the experiment, it was not possible to quantify the dynamic leakage directly. Instead, two observations from the experiment served to validate the zero leakage prediction. First, no visible leakage was seen during the piston ascending and descending periods, and second, the O-ring was leak free when the cylinder was loaded because no motion was observed for 24 h.

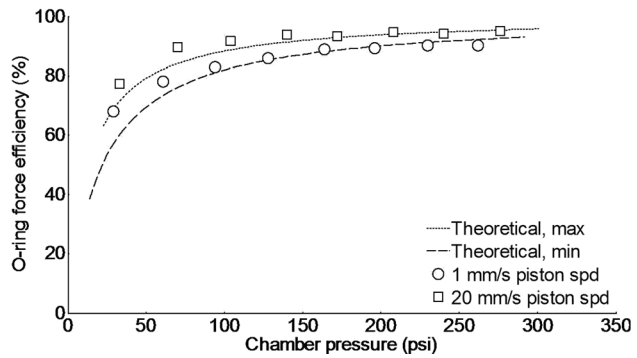

Fig. 5 Experimentally determined cylinder force efficiency as a function of pressure for two rod speeds. The lines are the predicted efficiency curves from the O-ring model for the extremes of the coefficient of friction.

To validate the calculation of estimated cylinder weight based on the theory presented in the previous sections, Eq. (17) was used to predict the weight of commercially available cylinders. Catalog data for 187 hydraulic cylinders from several manufacturers (Airpot, Beily, Bimba, Hercules, Prince) were used to build a database of rated pressure, bore, stroke and weight for real products. For the analysis, the cylinder material was assumed to be 304 stainless steel, which provided the yield strength, Young's modulus, Poisson's ratio and material density for the equations. (A real cylinder would be fabricated from several materials.) The safety factor N was set to 2 as this was the value found in two of the vendor catalogs. Common parameters were used for O-ring seal and hydraulic oil: 10% for squeeze ratio, 10 MPa for O-ring Young's modulus, 1 mm for O-ring seal cross-section diameter and 0.1 Pa·s for fluid viscosity. The pressure, bore, stroke, material properties and safety factor were used to calculate the theoretical wall thickness, volume and weight for the cylinder. The theoretical weight was then compared to the actual weight for the cylinder. Figure 7 shows the results. If the theory held for real cylinders exactly, all data points would lie on the solid line. The figure shows that real cylinders are somewhat lighter than their predicted weight for heavier cylinders, and somewhat heavier than their predicted weight for lighter cylinders (see inset.) The latter is likely because for the smallest cylinders, the weight of fittings and mounting hardware, not accounted for by the theory, become a significant fraction of the total weight.

3.2 Hydraulic Conduit. For smooth pipes, the approximate fluid flow equations are [18]

$$P_2 - P_1 = \frac{f_p \cdot \rho_f \cdot V_p^2 \cdot L_p}{2 \cdot D_p} \tag{18}$$

$$A_p = \frac{\pi \cdot D_p^2}{4} \tag{19}$$

$$V_p = \frac{Q_p}{A_p} \tag{20}$$

$$\text{Re} = \frac{\rho_f \cdot D_p \cdot V_p}{\mu} \tag{21}$$

$$f_p = \begin{cases} 64/\text{Re} & \text{laminar flow} \\ 0.316/\text{Re}^{0.25} & \text{turbulent flow} \end{cases} \tag{22}$$

where P_2 is pipe inlet pressure, P_1 is pipe outlet pressure, f_p is pipe friction coefficient, ρ_f is fluid density, V_p is pipe flow

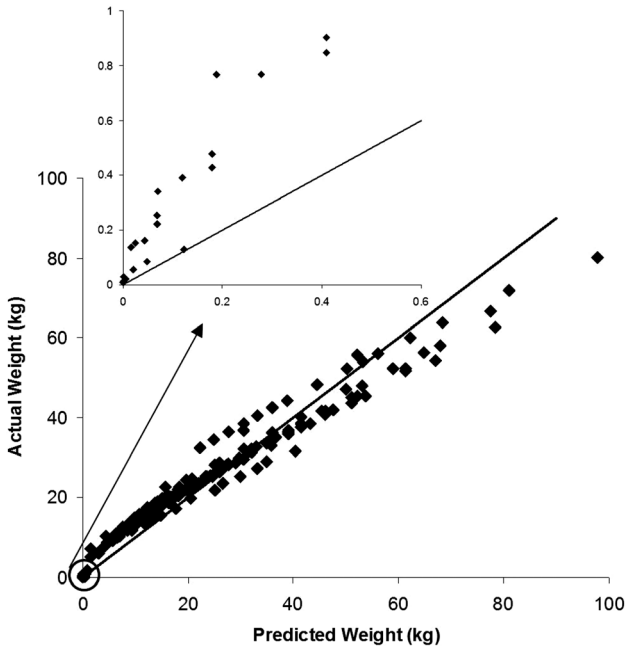

Fig. 7 Comparison between the actual weight and the weight predicted from the theoretical analysis for 187 commercial cylinders. The solid line indicates an exact match between actual and predicted. The inset expands the data for light weight cylinders.

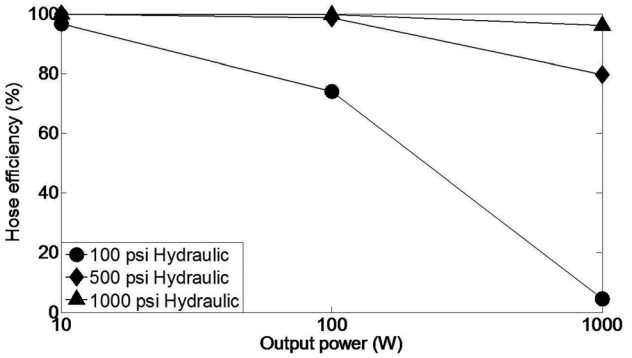

Fig. 8 Hydraulic conduit efficiency at several pressures and levels of output power, showing that the efficiency of the conduit is high unless the pressure is low. Conduit length: 1 m, conduit inner diameter: 5 mm.

velocity, L_p is pipe length, D_p is pipe inner diameter, A_p is pipe cross-section area, Q_p is pipe flow rate, and Re is the Reynolds number.

Using Eqs. (18)–(22), the pipe efficiency is

$$\eta_p = \frac{P_1}{P_2} = \begin{cases} 1 - \dfrac{128\mu}{\pi} \cdot \dfrac{Q_p \cdot L_p}{D_p^4 \cdot P_2} & \text{laminar} \\ 1 - \dfrac{1.79\mu^{0.25} \cdot \rho_f^{0.75}}{\pi^{1.75}} \cdot \dfrac{Q_p^{1.75} \cdot L_p}{P_2 \cdot D_p^{4.75}} & \text{turbulent} \end{cases} \tag{23}$$

These equations enable calculating the pipe i.d. D_p as a function of Q_p, L_p, P_2, and η_p.

The pipe weight can be calculated once the pipe wall thickness is found using the thin-walled cylinder formula [12]

$$t_5 = \frac{N \cdot P_2 \cdot D_p}{2S_y} \tag{24}$$

where t_5 is wall thickness, N is design safety factor, and S_y is pipe material yield strength. For this analysis we assumed that the pipes, like the cylinders, were fabricated from 304 stainless steel.

The weight of the pipe is

$$M_{\text{conduit}} = \pi\left(\left(\frac{D_p}{2} + t_5\right)^2 - \left(\frac{D_p}{2}\right)^2\right) L_p \rho_p \tag{25}$$

where ρ_p is the pipe density. The weight of the oil in the pipe is

$$M_{\text{ConduitOil}} = \pi\left(\frac{D_p}{2}\right)^2 L_p \rho_f \tag{26}$$

where ρ_f is the oil density.

The pipe efficiency η_p, inlet pressure P_2 and fluid flow rate Q_p were calculated using

$$\eta_p = \frac{\eta_{sys}}{\eta_{cyl}} \tag{27}$$

$$P_2 = \frac{P_1}{\eta_p} \tag{28}$$

$$Q_p = \frac{F_r \cdot V_r}{\eta_{sys} \cdot P_2} \tag{29}$$

where η_{sys} is the desired overall efficiency, η_{cyl} is the cylinder efficiency, F_r is rod force and V_r is rod velocity.

Figure 8 shows an example of the hydraulic conduit efficiency calculations. As expected, the efficiency of the hose only matters when running at high power and low pressure because under these conditions the flow rate is high, which results in a significant pressure drop. Our calculations (not shown) demonstrated that for most tiny hydraulic systems, the weight of the conduit is much smaller than the weight of the cylinder and can be ignored when doing approximate predictions of total system weight.

3.3 Hydraulic System Weight. Figure 9 illustrates how the weight of the hydraulic system is calculated. First, the output force, output velocity and stroke length are specified by the application requirements. Using this information, cylinder weight, efficiency, bore and rod diameter are calculated. Using the overall system efficiency of the equivalent electromechanical system, the hydraulic pipe inlet power and efficiency is calculated then hydraulic pipe inlet pressure is calculated for a given cylinder operating pressure. Next hydraulic pipe inlet flow rate is calculated using inlet power and pressure, then the hydraulic pipe diameter using inlet pressure, inlet flow rate, pipe efficiency and pipe length information, as shown in Eq. (23). With these numbers, pipe weight is calculated. Finally, total system weight is calculated by summing weights of the cylinder, pipe and hydraulic oil contained in the cylinder and pipe.

4 Electromechanical System Analysis

The electromechanical system includes wire for the transmission line, a DC electric motor and a ball screw. Unlike hydraulic components, electromechanical components for small-scale applications are readily available. Therefore, rather than using theoretical methods, the approach to estimating the total weight of an electromechanical solution was to develop a set of empirical equations that captured the scaling of component weight and efficiency with load or power based on the properties of high-end, commercially available electromechanical components captured from company catalogs.

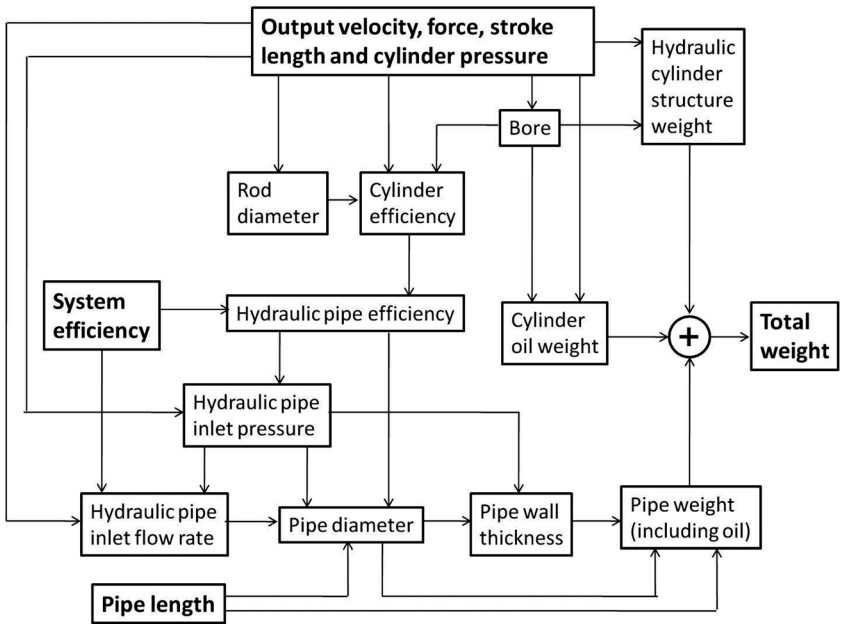

Fig. 9 Method for calculating the weight of a hydraulic system

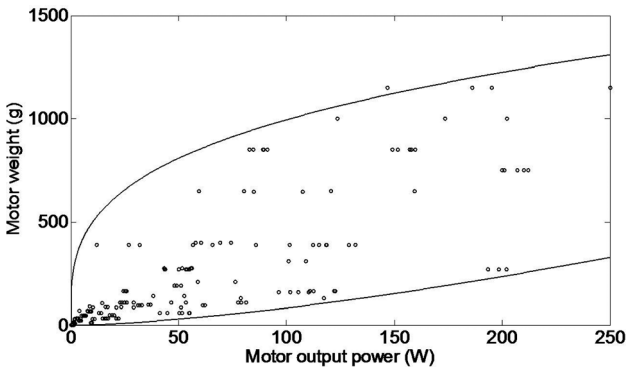

Fig. 10 Motor weight vs. output power

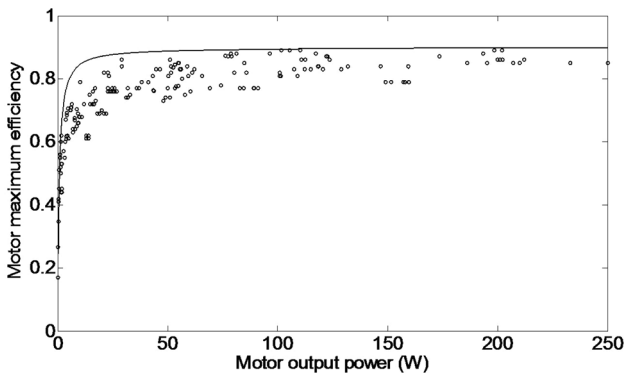

Fig. 11 Motor efficiency vs. output power

4.1 DC Electric Motor. The key system-level parameters for DC electric motors are weight and efficiency. Brushless, permanent magnet DC motors were chosen because for small precision applications they have the highest efficiency and highest power density. Power, weight and efficiency data for 192 motors from two manufacturers (MicroMo Electronics Inc. and Maxon Motor) were collected. The power for a motor was taken as the peak continuous mechanical output power and the efficiency was the electrical power in to mechanical power out maximum efficiency at the nominal voltage. Figure 10 plots motor weight versus motor power and Fig. 11 plots motor efficiency versus power for the motor data set.

For modeling purposes, empirical equations were created to bound motor properties. The lower curve in Fig. 10 is the lower bound of motor weight. Using this curve in a system analysis means that one is looking for the lightest available motor for a given power. The upper curve in Fig. 11 is the upper bound of motor efficiency. Using this curve in an a system analysis means that one is looking for the highest efficiency motor for a given power. The two bounding curves are

$$W_m = \frac{P_m^{1.5}}{12} \tag{30}$$

$$\eta_m = 0.9 - 0.9 \cdot \frac{0.1}{0.15 \cdot P_m + 0.1} \tag{31}$$

where W_m is motor weight, η_m is motor efficiency, and P_m is motor power.

4.2 Ball Screw. The ball screw converts the motor rotary power to low speed, high force linear power. The weight of a ball screw is related to its rated dynamic load and stroke length. Weight does not depend on rated velocity assuming the ball screw operates within its rated velocity. Rated dynamic load, stroke length, and weight data were collected from catalog data for 82 ball screws from one manufacturer (Nook Industries). Figure 12 shows weight as a function of rated load for two strokes, and an empirical equation for the lower bound of weight as a function of load and stroke was developed from the data

$$W_{\text{bs}} = F_{\text{bs}} \cdot \frac{180 + 3000 \cdot S_{\text{bs}}}{10000} \tag{32}$$

where W_{bs} is ball screw weight, F_{bs} is ball screw rated dynamic load, and S_{bs} is ball screw stroke length. The equation is the solid line in Fig. 12.

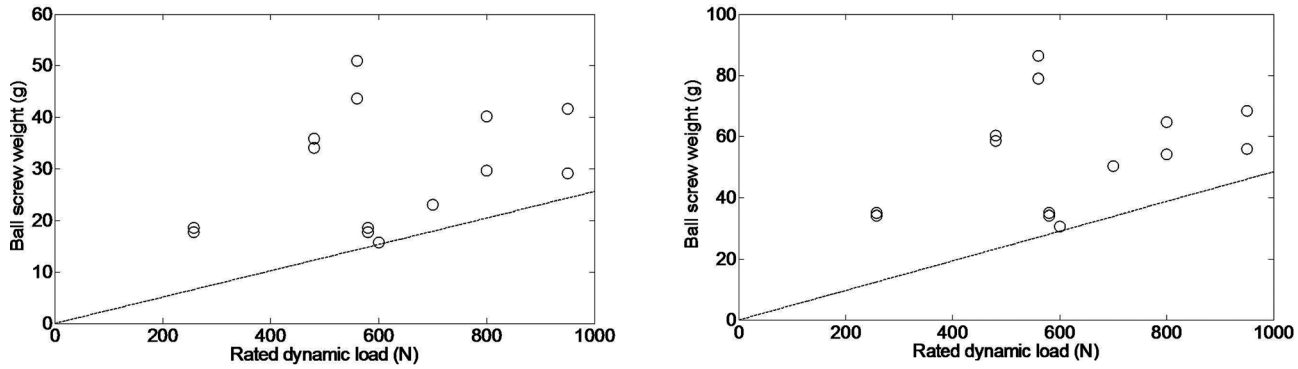

Fig. 12 Ball screw weight vs. rated dynamic load at.01 m (top) and.04 m (bottom) stroke

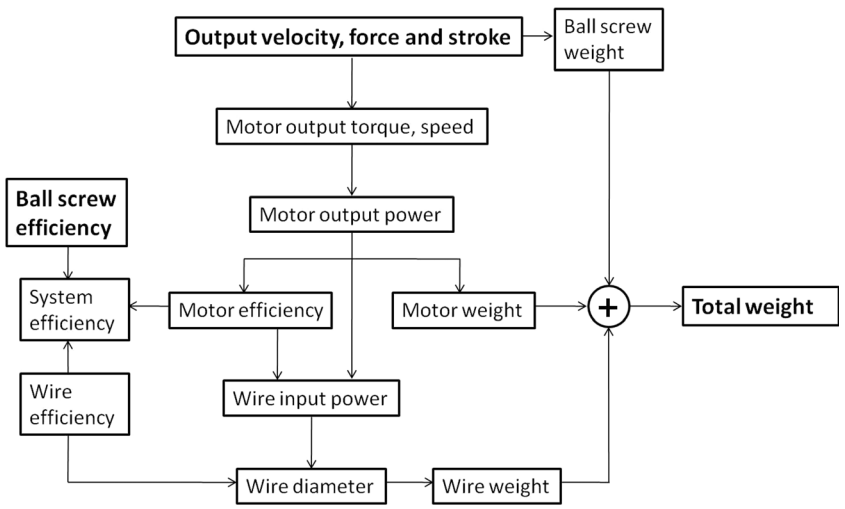

Fig. 13 Method for calculating the weight of an electromechanical system

The transmission equations for the ball screw are

$$T_m = F_{\text{bs}} \cdot \frac{L_{\text{bs}}}{2\pi} \cdot \frac{1}{\eta_{\text{bs}}} \tag{33}$$

$$\omega_m = \frac{V_{\text{bs}}}{L_{\text{bs}}} \tag{34}$$

where T_m is motor shaft torque, F_{bs} is ball screw force, L_{bs} is the transmission ratio, η_{bs} is ball screw efficiency, ω_m is motor shaft velocity, and V_{bs} is ball screw linear velocity. The ball screw efficiency was assumed to be 90%, which is typical for a high performance component. To simplify the electromechanical systems analysis, a fixed transmission ratio of 1 mm/rev was assumed for the ball screw.

4.3 Wire. The weight of wire can be significant when the wire is long, which would be the case when the battery is located some distance from the motor. High efficiency wire has large diameter but is heavy. The voltage drop across a length of electrical wire is [19]

$$\Delta U_{\text{w}} = \frac{4K_{\text{w}}}{\pi} \cdot \frac{P_w}{U_w} \cdot \frac{L_{\text{w}}}{D_{\text{w}}^2} \tag{35}$$

where K_{w} is wire specific resistance, P_w is wire input power, U_w is wire input voltage, L_w is wire length, and D_w is wire diameter. Thus, wire efficiency is

$$\eta_{\text{w}} = \frac{U_w - \Delta U_{\text{w}}}{U_w} = 1 - \frac{4K_{\text{w}}}{\pi} \cdot \frac{P_w}{U_w^2} \cdot \frac{L_{\text{w}}}{D_{\text{w}}^2} \tag{36}$$

High wire efficiency results in a large wire diameter and thus a large wire weight. In contrast, low wire efficiency means the wire must dissipate a considerable amount of thermal energy, which can melt the insulation. To prevent the system level weight optimization algorithm from suggesting either extreme, the wire efficiency was fixed at 99%, which is realistic for many systems.

Inverting (36) provides an equation for wire diameter

$$D_{\text{w}} = \sqrt{\frac{4K_{\text{w}}}{\pi} \cdot \frac{P_w}{U_w^2} \cdot \frac{L_{\text{w}}}{(1 - E_{\text{w}})}} \tag{37}$$

and the weight of the wire, without considering the insulation layer, is

$$W_{\text{w}} = \frac{\pi}{4} \cdot D_{\text{w}}^2 \cdot L_{\text{w}} \cdot \rho_{\text{w}} \cdot 1000 \tag{38}$$

where W_{w} is wire weight, and ρ_{w} is the density of the wire material. The analysis assumed copper wire with density 8960 kg/m^3 and specific resistance 17 nΩm.

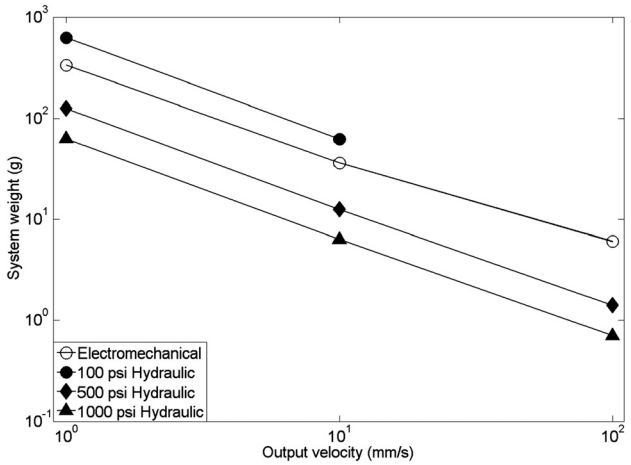

Fig. 14 Hydraulic and electromechanical system weight at several output velocities. Output power: 10 W, stroke: 0.05 m, transmission line length: 0.1 m. The 100 psi, 100 mm/s data point is missing because there is no low pressure, high speed hydraulic system that can match the efficiency of the equivalent electromechanical system.

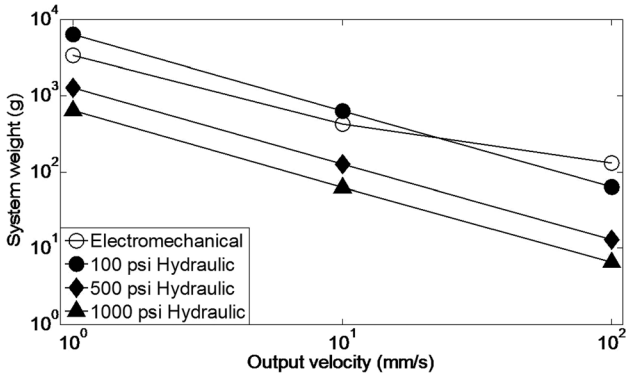

Fig. 15 Hydraulic and electromechanical system weight at several output velocities. Output power: 100 W, stroke: 0.05 m, transmission line length: 0.1 m.

4.4 Electromechanical System Weight. Figure 13 illustrates the approach for calculating the weight of the electromechanical solution. The application requirements set the ball screw output velocity, force and stroke. The ball screw weight is then calculated using (32). The electric motor shaft power is calculated from

$$P_m = \frac{T_m}{1000} \cdot 2\pi \cdot \omega_m = \frac{F_{\text{bs}} \cdot V_{\text{bs}}}{\eta_{\text{bs}}} \tag{39}$$

using Eqs. (33) and (34). This determines the motor weight and efficiency according to Eqs. (30) and (31). Next, the input power to the wire is determined from

$$P_w = P_m \cdot \frac{1}{\eta_{\text{m}}} \cdot \frac{1}{\eta_{\text{w}}} \tag{40}$$

and then the wire diameter and wire weight are calculated from Eqs. (37) and (38). The system weight is the sum of the ball screw, motor, and wire weights. The overall electromechanical system efficiency is

$$\eta_{\text{esys}} = \eta_{\text{bs}} \cdot \eta_{\text{m}} \cdot \eta_{\text{w}} \tag{41}$$

5 Method to Compare Hydraulic and Electromechanical Systems

With the ability to calculate hydraulic and electromechanical system weight and efficiency for a given application the two realizations can be compared to determine which will be lighter. The method used for the comparison was to: (1) Establish the design problem by specifying a system force and power (or force and velocity), and linear excursion. (2) Design an electromechanical solution using the empirical bounding equations as a stand-in for the best-available DC brushless motor and ball screw. (3) Calculate the efficiency of the resulting electromechanical system. (4) Design a comparable hydraulic system with the same force, power and stroke design requirements and the same efficiency. (5) Calculate and compare the weights of the electromechanical and hydraulic solutions. An application was implemented in MATLAB to facilitate the calculations.

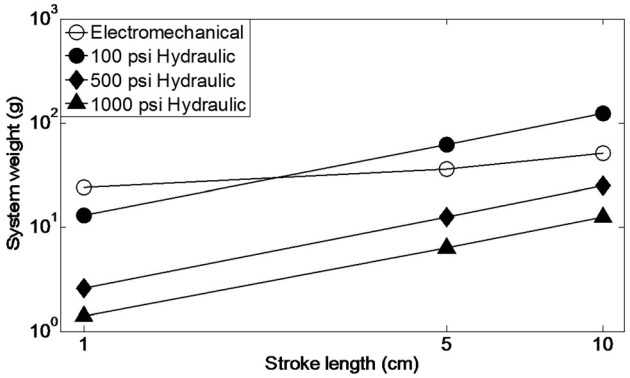

Fig. 16 Hydraulic and electromechanical system weight at several stroke lengths. Output power: 10 W, velocity: 0.01 m/s, transmission line length: 0.1 m.

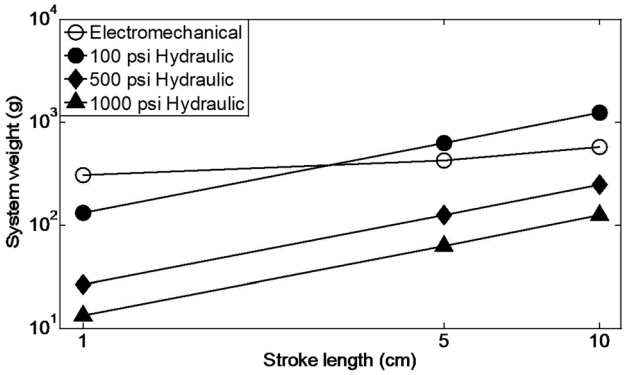

Fig. 17 Hydraulic and electromechanical system weight at several stroke lengths. Output power: 100 W, velocity: 0.01 m/s, transmission line length: 0.1 m.

6 Results

Weight comparison examples are shown in Figs. 14–21. Figures 14–19 show system weight for a mechanical output power of 100 W and 10 W for various configurations of velocity, stroke length and transmission line length. The nominal voltage for the motors in the database ranged from 6 to 48 V but for this analysis 24 V motors were used. Motor voltage has some, but not a significant effect on the electromechanical system weight because as the voltage decreases, the system weight will increase due to the wire diameter increasing to accommodate the increase in current at the same efficiency.

Operating pressure has a significant influence on the weight of a hydraulic system. Figure 20 shows the weights of hydraulic systems running at three pressures compared to the weight of the equivalent electromechanical system for three output power conditions with an output velocity of 10 mm/s. The 100 psi hydraulic

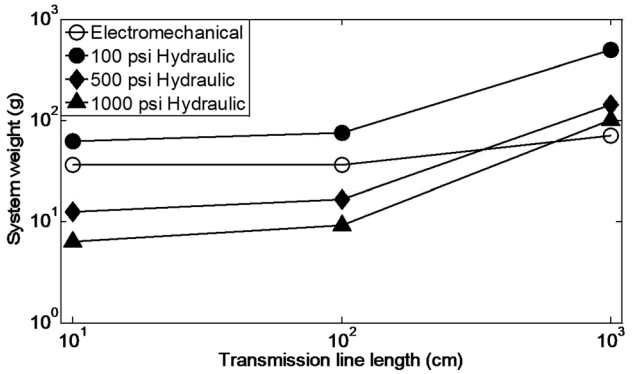

Fig. 18 Hydraulic and electromechanical system weight at several transmission line lengths. Output power: 10 W, stroke: 0.05 m, velocity: 0.01 m/s.

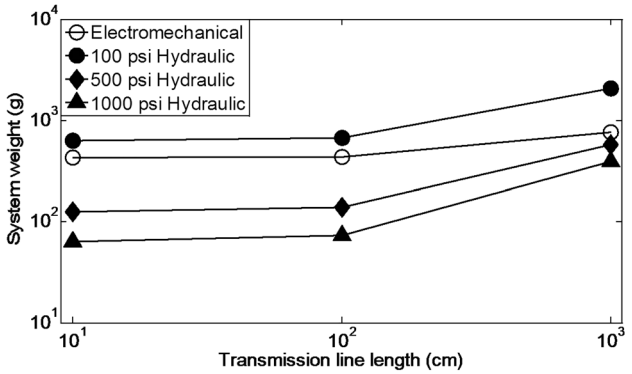

Fig. 19 Hydraulic and electromechanical system weight at several transmission line lengths. Output power: 100 W, stroke: 0.05 m, velocity: 0.01 m/s.

system is heavier than the equivalent electromechanical system while the 500 psi and 1000 psi systems are lighter. Figure 21 shows the operating pressure required for the hydraulic system to have the same weight as the equivalent electromechanical system for three output powers. Pressures higher than the line will result in a lighter hydraulic system and pressures below the line will result in a heavier hydraulic system.

7 Design Example

A powered ankle foot orthosis (AFO) is a device that helps people with muscle deficiency to lift their toe or push off while walking [20]. The AFO was chosen as the design example because of its challenging requirements. Large torque and large power is required during the push off phase of gait but the weight of the AFO on the ankle must be less than 2 kg to not influence leg swing dynamics. Figure 22 shows ankle torque and velocity for one step when walking at normal speed. The vertical dotted-dashed line marks the point during the gait cycle where the ankle produces maximum power with torque 90 Nm and velocity 100 deg/s. This occurs just before toe-off and the AFO was designed to match this power.

Figure 23 shows the placement of a single hydraulic cylinder for the conceptual design of a powered AFO. The cylinder is oriented to extend for ankle plantar flexion to take advantage of the larger cap side piston area compared to the rod side. To reduce the AFO package size, in the neutral position, a moment arm of 8 cm was assumed. The ankle range of motion is 20 deg in dorsi-flexion and 50 deg in plantar-flexion for a total of 70 deg [22]. To minimize the weight carried on the ankle, the hydraulic power supply

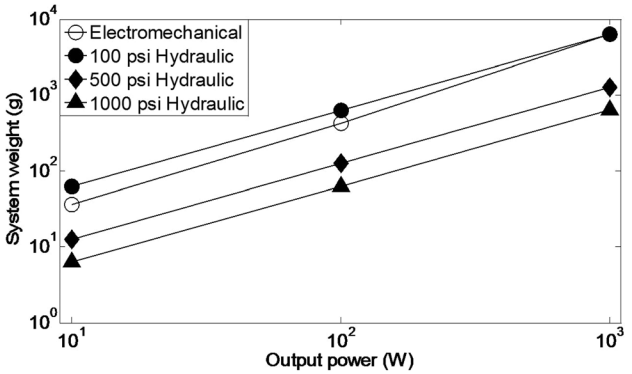

Fig. 20 Hydraulic and electromechanical system weight at several output powers. Stroke: 0.05 m, velocity: 0.01 m/s, transmission line length: 0.1 m.

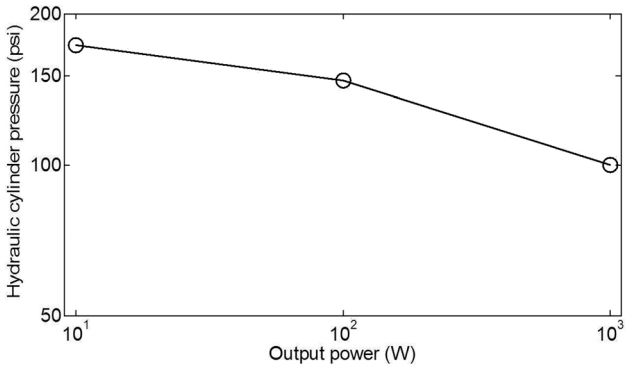

Fig. 21 Operating pressure required for the hydraulic system to be the same weight as the equivalent electromechanical system at several output powers. Stroke: 0.05 m, velocity: 0.01 m/s, transmission line length: 0.1 m.

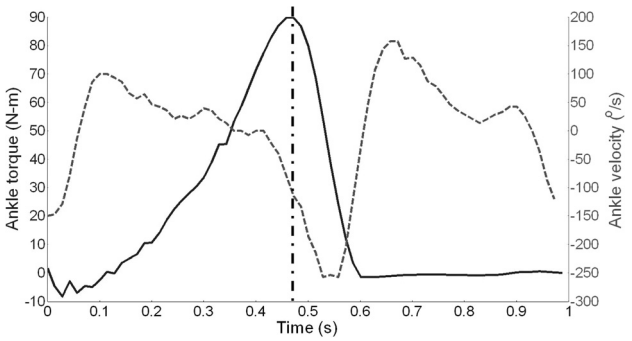

Fig. 22 Ankle torque (solid) and velocity (dashed) for one step when walking at normal speed. The vertical dotted-dashed line marks the peak power point. Data from Ref. 21.

was assumed to be carried at the waist, separated from the actuator by a 1 m hydraulic hose.

The cylinder stroke length, maximum output force, maximum output velocity and maximum output power were derived from the geometry

$$S = S_f - S_i \tag{42}$$

$$S_i = \sqrt{a^2 + b^2 - 2 \cdot a \cdot b \cdot \cos(\theta_i)} \tag{43}$$

$$S_f = \sqrt{a^2 + b^2 - 2 \cdot a \cdot b \cdot \cos(\theta_f)} \tag{44}$$

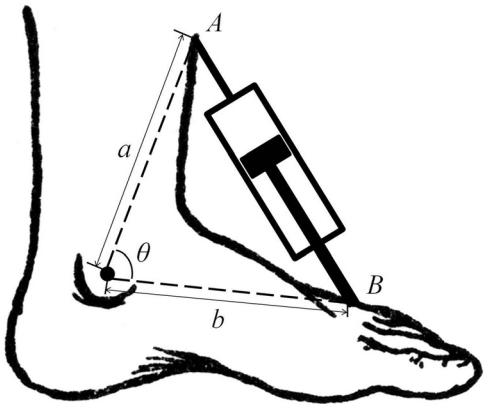

Fig. 23 Conceptual design for a hydraulic AFO.

Table 3 AFO systems weight comparison

System	Component	Wt (g)	Total Wt (g)
Electromechanical	Ball screw	44	
	DC motor	192	241
	Wire	5	
200 psi hydraulics	Cylinder	210	248
	Hoses	38	
500 psi hydraulics	Cylinder	106	125
	Hoses	19	

$$F_{\max} = \frac{T_{\max}}{L_{\mathrm{ma}}} \tag{45}$$

$$V_{\max} = \frac{\Omega_{\max}}{180\,\mathrm{deg}} \cdot \pi \cdot L_{\mathrm{ma}} \tag{46}$$

$$\mathrm{POW}_{\max} = T_{\max} \cdot \Omega_{\max} \tag{47}$$

where S_i and S_f are the initial and final distance between the cylinder mounting point A and B (Fig. 23), $\theta_i = 70\,\mathrm{deg}$ and $\theta_f = 140\,\mathrm{deg}$ are the ankle angles corresponding to S_i and S_f, and a and b are fixed at 10 cm.

The system specifications from Eqs. (42) to (47) were used in Eqs. (1)–(41) along with the methods described in Sec. 5 to compute the theoretical weight of the electromechanical and hydraulic AFO components for the design example. The results are shown in Table 3. At 200 psi, the hydraulic system will be about the same weight as the equivalent electromechanical system but at 500 psi, it will be about one half the weight. While the 500 psi cylinder and hose must have thicker walls to accommodate the higher pressure, the bore size to achieve the same force is smaller at 500 psi resulting in overall lighter components.

8 Discussion

The key result of this study is that for applications where the output power is less than 100 W a hydraulic solution will be lighter than the equivalent electromechanical solution only if the hydraulics runs at high pressure. For example, Fig. 20 shows that a 100 W electromechanical system is predicted to weigh 428 g while a 100 W hydraulic system running at 1000 psi is predicted to weigh 63 g, about seven times lighter. While the exact numbers are system dependent (for example, as the power source is placed further away, the drag in small hydraulic lines becomes significant,) the conclusion is clear: for tiny, light hydraulic systems the operating pressure must be high.

There is an upper limit on the pressure. For equal force, the higher the pressure the smaller the bore of the cylinder but Fig. 4 shows that efficiency rapidly drops if the bore becomes too small. Low efficiency is problematic because a large, heavy power source is needed to provide the energy required by the application and because the wasted energy results in heating that cannot be carried away by the tiny amount of circulating fluid. Thus, efficiency considerations lead to an effective lower limit on size, about 4 mm, and therefore an upper limit on pressure.

Because tiny high pressure hydraulic components are not available, small hydraulic systems are currently run at low pressures, often using pneumatic components that are small and light but generally limited to about 200 psi. (One exception is the small custom cylinder for the prototype prosthetic finger by Love [5].) Thus, there is a need for small components that operate at high pressures and are at the weight predicted by Eqs. (17) and (25).

The limitation of this study is that it ignores the power supply and control means, which are significant components of the complete system. Analyzing only the distal components still provides guidance to the designer for two reasons. First, it is often the distally mounted components that are most weight sensitive and second, including the power supply and control would not change the main conclusion which is that tiny hydraulics should be run at high pressure to minimize weight.

Turning to the complete hydraulic system, hydraulic power supplies are typically large and heavy and traditional throttling control valves are inefficient. For truly lightweight, low power, mobile systems such as powered hand tools and powered orthotics, compact sources of high pressure fluid using pumps driven by battery powered electric motors or by tiny, high power density internal combustion engines are needed. Tiny cartridge piston pumps are available but have a modest efficiency of about 30% at 500 psi. There is also a need for tiny, high pressure, low flow hydraulic control valves that operate in an efficient on–off switching mode. The common PWM drivers for electric motors are efficient but have no equivalent in fluid power. Low-pressure, low flow digital MEMS valves are used in microfluidics, but are not suitable for transmitting power in the one to 100 W range.

Other problems with tiny hydraulics for human-scale applications that must be solved include leakage of oil into the environment, which calls for developing low friction, leakless seals; cavitation of the fluid, which may be a significant problem for oil running through small passages at low pressure and high velocity; and creating designs that integrate structure, conduit, valving and cylinders to minimize weight by eliminating fittings.

Acknowledgment

Students at the Georgia Institute of Technology under the direction of Professor Chris Paredis created the database of hydraulic cylinder properties. Undergraduate Ellen Weburg made substantial contributions to the seal testing experiments. This research was supported by the Center for Compact and Efficient Fluid Power, a National Science Foundation Engineering Research Center, funded under cooperative Agreement No. EEC-0540834.

References

[1] Hunt, T., and Vaughan, N., 1996, *The Hydraulic Handbook*, 9th ed., Elsevier Science, Oxford, UK.
[2] Pippenger, J., and Hicks, T., 1979, *Industrial Hydraulics*, 3rd ed., McGraw-Hill, New York.
[3] Dollar, A., and Herr, H., 2008, "Lower Extremity Exoskeletons and Active Orthoses: Challenges and State-of-the-Art," IEEE Trans. Rob., **24**(1), pp. 1–15.
[4] Yang, C., Zhang, J., Chen, Y., Dong, Y., and Zhang, Y., 2008, "A Review of Exoskeleton-Type Systems and Their Key Technologies," Proc. IMechE Part C: J. Mech. Eng. Sci., **222**, pp. 1599–1612.
[5] Love, L., Lind, R., and Jansen, J., 2009, "Mesofluidic Actuation for Articulated Finger and Hand Prosthetics," IEEE International Conference on Intelligent Robots and Systems, pp. 2586–2591.
[6] Peris, J., Reynaerts, D., and Brussel, H., 2000, "Design of Miniature Parallel Manipulators for Integration in a Self-Propelling Endoscope," Sens. Actuators, **85**, pp 409–417.
[7] Volder, M., Ceyssens, F., and Reynaerts, D., 2007, "A PDMS Lipseal for Hydraulic and Pneumatic Microactuators," J. Micromech. Microeng., **17**(7), pp. 1232–1237.

[8] Volder, M., and Reynaerts, D., 2009, "Development of a Hybrid Ferrofluid Seal Technology for Miniature Pneumatic and Hydraulic Actuators," Sens. Actuators, A, **152**, pp. 234–240.
[9] Laser, D., and Santiago, J., 2004, "A Review of Micropumps," J. Micromech. Microeng., **14**(6), pp. R35–R64.
[10] Oh, K., and Ahn, C., 2006, "A Review of Microvalves," J. Micromech. Microeng. **16**(5), pp. R13–R39.
[11] Volder, M., and Reynaerts, D., 2010, "Pneumatic and Hydraulic Microactuators: A Review," J. Micromech. Microeng., **20**(4), p. 043001.
[12] Kannappan, P., 1986, *Introduction to Pipe Stress Analysis*, John Wiley & Sons, New York, pp. 22–29.
[13] Myer, K., 1998, *Mechanical Engineers' Handbook*, 2nd ed., John Wiley & Sons, New York, pp 229–242.
[14] Manring, H., 2005, *Hydraulic Control Systems*, John Wiley & Sons, New York.
[15] Al-Ghathian, F., and Tarawneh, M., 2005, "Friction Forces in O-Ring Sealing," Am. J. Appl. Sci., **2**(3), pp. 626–632.
[16] Karaszkiewicz, A., 1990, "Geometry and Contact Pressure of an O-Ring Mounted in a Seal Groove," Ind. Eng. Chem. Res., **29**(10), pp. 2134–2137.
[17] Karaszkiewicz, A., 1998, "Hydrodynamic Lubrication of Rubber Seals for Reciprocating Motion; Leakage of Seals With an O-ring," Tribol. Int., **21**(6), pp. 361–367.
[18] Young, D., Munson, B., and Okiishi, T., 1997, *A Brief Introduction to Fluid Mechanics*, John Wiley & Sons, New York.
[19] Singer, B., and Forster, H., 1990, *Basic Mathematics for Electricity and Electronics*, 6th ed., McGraw-Hill, New York, pp. 370–398.
[20] Shorter, K., Xia, J., Hsiao-Wecksler, E., Durfee, W., and Kogler, G., 2012, "Technologies for Powered Ankle-Foot Orthic Systems: Possibilities and Challenges," IEEE/ASME Trans. Mechatron., **18**(1), pp. 337–347.
[21] Winter, D., 2005, *Biomechanics and Motor Control of Human Movement*, 3rd ed., John Wiley & Sons, New York.
[22] Hamilton, N., Weimar, W., and Juttgens, K., 1997, Kinesiology; Scientific Basis of Human Motion, 11th ed., McGraw-Hill, New York.